ORGANOMETALLICS

Article

pubs.acs.org/Organometallics

Elucidating Dramatic Ligand Effects on SET Processes: Iron Hydride versus Iron Borohydride Catalyzed Reductive Radical Cyclization of Unsaturated Organic Halides

Sara H. Kyne,[†,⊥] Martin Clémancey,[‡] Geneviève Blondin,[‡] Etienne Derat,[†] Louis Fensterbank,*[,†] Anny Jutand,*[,§] Guillaume Lefèvre,*[,∥] and Cyril Ollivier*[,†]

[†]Sorbonne Universités, UPMC Univ Paris 06, CNRS, UMR 8232, Institut Parisien de Chimie Moléculaire, 4 place Jussieu, F-75252 Paris Cedex 05, France

[‡]Université Grenoble Alpes, CEA, CNRS, LCBM (UMR 5249), pmb, F-38000 Grenoble, France

[§]Ecole Normale Supérieure-PSL Research University, Département de Chimie, Sorbonne Universités, UPMC Univ Paris 06, CNRS UMR 8640 PASTEUR, 24 Rue Lhomond, F-75231 Paris Cedex 05, France

[∥]NIMBE, CEA, CNRS, Université Paris-Saclay, Gif-sur-Yvette, France

Supporting Information

ABSTRACT: An iron(II) borohydride complex ($[(\eta^1\text{-}H_3BH)\text{-}FeCl(NCCH_3)_4]$) is employed as the precatalyst in iron-catalyzed radical cyclizations of unsaturated organic halides in the presence of $NaBH_4$. Mechanistic investigations have established that the ligand bound to the metal center (acetonitrile versus ethylenebis(diphenylphosphine) (dppe)) plays a crucial role in the structure and reactivity of the active anionic iron(I) hydride ($[HFeCl(dppe)_2]^-$) and borohydride ($[(\eta^1\text{-}H_3BH)FeCl(NCCH_3)_4]^-$) with unsaturated haloacetals. This work provides new insights into iron(I) hydride and borohydride species and their potential implication in single-electron processes.

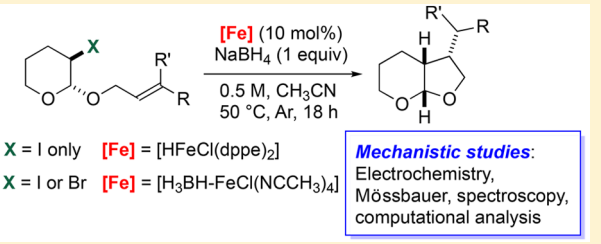

INTRODUCTION

Transition metals have been widely employed in radical chemistry[1] since the pioneering works of Kochi and co-workers, which documented the importance of single-electron-transfer (SET) processes in such metal-catalyzed reactions.[2] Particularly, transition-metal complexes with low oxidation state readily undergo reduction of organic substrates to form a variety of carbon-centered radicals under the appropriate reaction conditions.[3] Among these, it has been proposed that metal hydride complexes, which have proven their efficiency in catalysis and organic synthesis,[4] generate low-valent transition-metal hydride species under reducing conditions, acting as both mediators and hydrogen donors for reductive radical reactions with organic halides. However, the in situ formation of the transition-metal hydride species, generated from the corresponding metal-halogenated complexes and a stoichiometric amount of hydride source ($LiAlH_4$, $NaBH_4$, $NaBH_3CN$, Red-Al), and the subsequent reaction mechanism have both remained largely unexplored. Such radical transformations have been performed with metal complexes of gallium,[5] indium,[6] zirconium,[7] or titanium.[8] While plausible mechanisms for these reactions have been proposed, tangible evidence is still anecdotal. For instance, Oshima and co-workers used commercially available Schwartz reagent (bis(cyclopentadienyl)zirconium(IV) chloride hydride) as a stoichiometric reducing reagent, or catalytic reaction conditions of 20 mol % $[Cp_2ZrCl_2]$ in the presence of Red-Al, and Et_3B to promote reductive radical cyclization reactions of haloacetals. The authors proposed that the zirconium hydride (Zr−H) species was formed in situ from $[Cp_2ZrCl_2]$ in the presence of the strong reducing agent and acted as the precatalyst for the reaction. Hydrogen atom abstraction would give rise to the active zirconium(III) radical which undergoes SET with the substrate.[7] In one of the earliest examples of this chemistry, Schwartz employed substoichiometric $[Cp_2TiCl_2]$ in the presence of a large excess of sodium borohydride for an aryl halide reductive cyclization reaction (Scheme 1). Mechanistic studies were carried out on the titanium borohydride complex $[Cp_2Ti(BH_4)]$ which was presumably formed under the reaction conditions. A titanium hydride amine complex ($Cp_2Ti^{III}H$·amine) was suggested to be responsible for electron transfer. Evidence of this species was circumstantial but showed that the rate of cleavage of the Ti−HBH_3 bond varied in the presence of different amines such as pyridine and *N*,*N*-dimethylethylamine.[8] These studies led to the conclusion that metal hydride and borohydride complexes can both act as precatalysts of the reduction reaction of organic halides

Special Issue: Organometallic Chemistry in Europe

Received: August 5, 2017

DOI: 10.1021/acs.organomet.7b00603
Organometallics XXXX, XXX, XXX−XXX

Scheme 1. Transition-Metal-Mediated Radical Reactions and Postulated Intermediates Formed in Situ

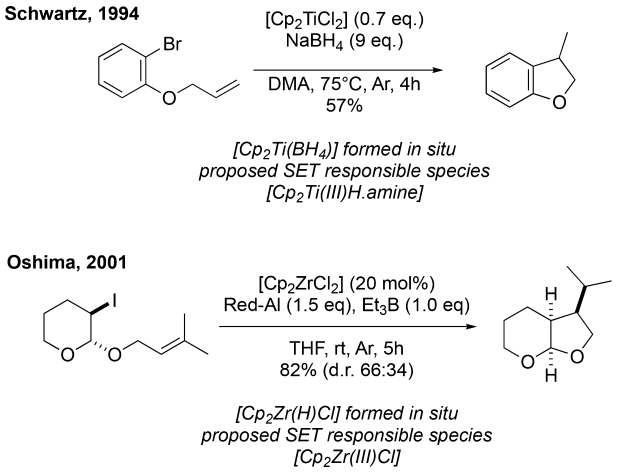

depending on the nature of the metal and potentially also the ligand.

Iron is reactive in redox chemistry: in particular, an array of reduction reactions has been carried out in the presence of metal reducing agents. Thanks principally to the pioneering work by Kharash and Kochi, iron catalysts have been exploited in a broad range of cross-coupling reactions of alkyl halides with Grignard reagents.[9] Meunier and co-workers first reported that a stoichiometric amount of an iron−magnesium complex (Cp(DIPHOS)FeMgBr) mediated the 5-exo radical cyclization reaction of 5-hexenyl bromide.[10] Oshima and co-workers developed intramolecular radical cyclization reactions of haloacetals in the presence of 5 mol % of iron(II) dichloride and a stoichiometric Grignard reagent as the reducing agent.[11] Other iron-mediated reduction reactions have also been developed,[12] and particularly, other mixed iron(II) or iron-(III)/hydride systems have also been applied to several different radical transformations.[13]

Over the last 50 years, various iron monohydride[14] and borohydride[15] complexes have been reported in the literature, but their use in radical synthesis remains scarce.

In an initial communication, we reported a novel 5-exo cyclization of 2-allyloxy-3-halotetrahydropyrans ($\mathbf{1_I}$, $\mathbf{1_{Br}}$) in the presence of iron(II) dichloride and sodium borohydride (Scheme 2).[16]

Scheme 2. Reaction of Haloacetals (1) in the Presence of Iron(II) Complexes and $NaBH_4$

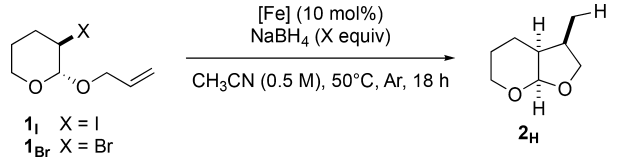

As shown in Table 1, iron(II) dichloride (10 mol %) promoted the reaction of haloacetals ($\mathbf{1_I}$, $\mathbf{1_{Br}}$) in the presence of excess sodium borohydride (1.5 equiv) to give 73% and 78% yields of the bicyclic product ($\mathbf{2_H}$), respectively (Table 1, entries 1 and 2). Reaction of iodoacetal ($\mathbf{1_I}$) was also complete in the presence of $[HFeCl(dppe)_2]$[17] (**3**) and sodium borohydride (1 equiv) and provides support that an iron(II) hydride complex is a precatalyst for this reaction (Table 1, entry 3). Interestingly, no reaction was observed with the dihydride counterpart, $[H_2Fe(dppe)_2]$.

Table 1. Reactivity of 1 in the Presence of [Fe] (10 mol %) and $NaBH_4$[a]

entry	substrate	[Fe]	$NaBH_4$ (equiv)	yield (%)
1	$\mathbf{1_I}$	$FeCl_2$	1.50	73[b]
2	$\mathbf{1_{Br}}$	$FeCl_2$	1.50	78[b]
3	$\mathbf{1_I}$	$[HFeCl(dppe)_2]$	1.00	70[c]
4	$\mathbf{1_{Br}}$	$[HFeCl(dppe)_2]$	1.00	0

[a]Reaction conditions: **1** (1.0 mmol, 0.5 M in CH_3CN), [Fe] (10 mol %), $NaBH_4$ (X equiv), 50 °C, 18 h. [b]dr = 87:13. [c]dr = 90:10.

Electrochemical studies of $[HFe^{II}Cl(dppe)_2]$ (**3**) identified that an anionic iron(I) hydride species, $[HFe^{I}Cl(dppe)_2]^-$ ($\mathbf{3^-}$), was electrogenerated or formed in the presence of $NaBH_4$. This species ($\mathbf{3^-}$) was the active catalyst for the reaction, activating iodoacetal ($\mathbf{1_I}$) by electron transfer (SET) and regenerating the precatalyst in a catalytic cycle (Scheme 3).

Scheme 3. Electrochemical Generation of $[HFe^{I}Cl(dppe)_2]^-$ ($\mathbf{3^-}$) and Electron Transfer (SET) to $\mathbf{1_I}$

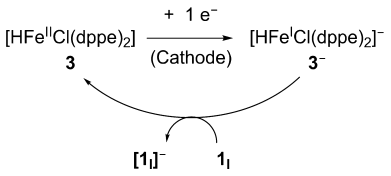

As shown in Scheme 4, during followup investigations we discovered that bromoacetal ($\mathbf{1_{Br}}$), in contrast to iodoacetal ($\mathbf{1_I}$), was completely unreactive in the presence of $[HFeCl(dppe)_2]$ (**3**) (Table 1, entry 4).[16b]

Scheme 4. No Reaction of Bromoacetal ($\mathbf{1_{Br}}$) in the Presence of $[HFeCl(dppe)_2]$ (3) and $NaBH_4$

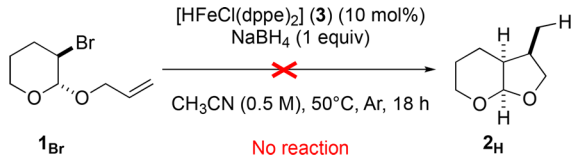

Herein, we report in detail the explanation for the lack of reactivity of $[HFe^{I}Cl(dppe)_2]^-$ with bromoacetal ($\mathbf{1_{Br}}$) and our investigation to better understand the important factors that determine the reactivity of iron hydride complexes. We have elucidated the crucial role played by the ligand, thus giving new insights into the reactivity of iron hydride complexes to mediate radical cyclization reactions. To our knowledge, no detailed mechanistic investigations have been reported on iron-mediated radical reactions involving the in situ formation of an iron hydride versus borohydride species in acetonitrile. In this article we discuss our efforts to expand the understanding of iron-mediated reductive radical reactions.

RESULTS AND DISCUSSION

Synthesis and Characterization of Iron(II) Bis-Chloride Complexes in Acetonitrile. As previously mentioned, an iron(II) hydride complex ($[HFeCl(dppe)_2]$ (**3**)) serves as a precatalyst for reductive 5-exo radical cyclization reactions. This structurally defined complex can be easily synthesized from

DOI: 10.1021/acs.organomet.7b00603
Organometallics XXXX, XXX, XXX−XXX

iron(II) dichloride upon reaction with sodium borohydride and dppe.[17] This led us to consider the identity of the precatalyst formed in situ from the same source of iron(II) in the presence of sodium borohydride in acetonitrile in the absence of any phosphine ligand. Acetonitrile is usually considered as a pure σ-donor ligand and will readily fill vacant metal coordination sites to provide stability in solution.[18] Indeed, literature reports supported the formation of iron−acetonitrile species. These complexes have even been isolated and characterized; however, their chemistry has not been greatly explored.[19]

Miller and co-workers have reported the solvation of iron(II) dichloride with acetonitrile to give an isolated species.[20] The crystal structure revealed the 1D chain polymer dichlorobis(acetonitrile)iron(II) ($\{Fe(\mu\text{-}Cl)_2(NCCH_3)_2\}_n$ (**4**)). This species was first described in 1964 by Hathaway and Holah and characterized by IR spectroscopy and titration.[19a] A procedure to synthesize the dichlorotetrakis(acetonitrile)iron(II) complex $FeCl_2(NCCH_3)_4$ is also available.[21]

The dichlorobis(acetonitrile)iron(II) complex ($\{Fe(\mu\text{-}Cl)_2(NCCH_3)_2\}_n$ (**4**)) was synthesized following the procedure reported by Miller and co-workers, giving off-white crystals in 85% yield (Scheme 5).[20] The X-ray structure matched the

Scheme 5. Synthesis of $\{Fe(\mu\text{-}Cl)_2(NCCH_3)_2\}_n$ (4)

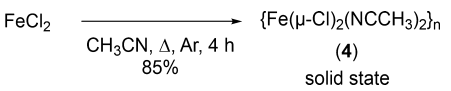

literature data. In this chain, an octahedral environment is accommodated by the iron centers, with bridging chloride anions and acetonitrile molecules in an apical position.

High-resolution ESI mass spectrometry revealed the presence of $[FeCl(NCCH_3)_2]^+$, a fragment resulting from the loss of one chloride ligand in the unit motif of the monomer (calcd 172.95634, found 172.95654).

The Mössbauer spectrum recorded at 80 K on a powder sample of $\{Fe(\mu\text{-}Cl)_2(NCCH_3)_2\}_n$ (**4**) (natural abundance in ^{57}Fe) reveals three doublets. The major doublet (64%) has nuclear parameters that are characteristic of high-spin (S = 2) Fe^{II} (δ = 1.24 mm s^{-1}, ΔE_Q = 2.07 mm s^{-1}). The isomer shift value is in agreement with that previously determined for an analogous 1D chain.[22] The second doublet (δ = 1.20 mm s^{-1}, ΔE_Q = 1.34 mm s^{-1}, contribution 26%) also exhibits nuclear parameters featuring a high-spin Fe^{II} ion. The two species differ in the quadrupole splitting values, suggesting that the two molecules of acetonitrile may be in either the trans or cis positions. The third doublet (δ = 0.34 mm s^{-1}, ΔE_Q = 1.12 mm s^{-1}, contribution 10%) presents nuclear parameters that are close to those of the tetrahedral ferric ion in $[N_6Fe^{III}-(\mu\text{-}O)-Fe^{III}Cl_3]^+$,[23] suggesting a slight contamination by the diferric μ-oxo species $[Cl_3Fe-(\mu\text{-}O)-FeCl_3]^{2-}$.

In order to investigate more closely the nature of the transient iron species generated in situ in the catalytic cyclization described in this work (Scheme 2), Mössbauer spectra of frozen solutions containing ^{57}Fe-enriched samples were recorded. First, $\{^{57}Fe(\mu\text{-}Cl)_2(S)_2\}_n$ (S = $NCCH_3$) was synthesized following Miller's procedure, at 0.05 M concentration to mimic the cyclization conditions (Scheme 5). An aliquot of this solution was frozen without preliminary purification, and the Mössbauer spectrum was recorded at 80 K. Most of the spectrum (ca. 90% of the total area) could be simulated with two quadrupole doublets (I and II, Figure 1a)

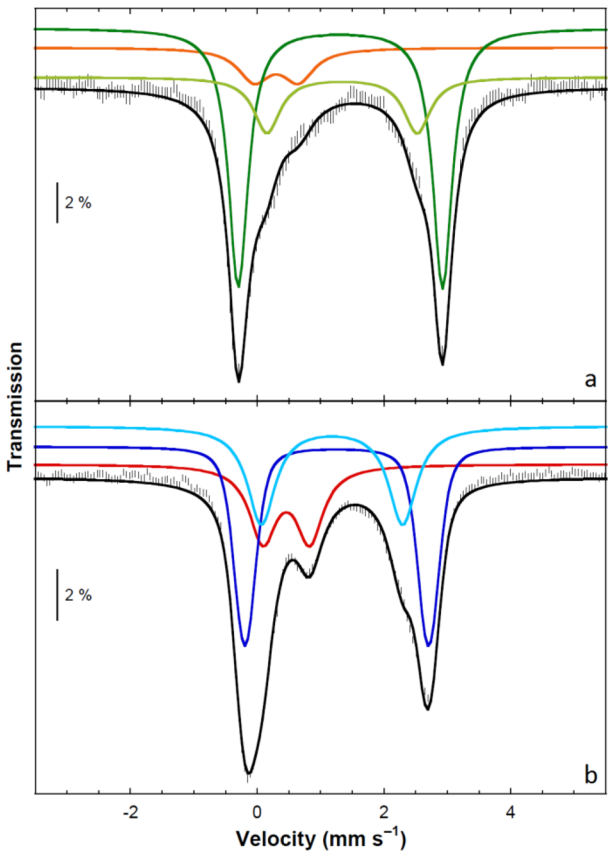

Figure 1. Zero-field Mössbauer spectra recorded at 80 K on acetonitrile solutions of $^{57}FeCl_2$ before (a) and after (b) the addition of 53 equiv of $NaBH_4$. Experimental data are shown as hatched bars, and simulations are overlaid as solid black lines. Contributions are shown in color as upper traces. See text and Table 2 for parameters.

characteristic of two high-spin Fe^{II} species (S = 2) featuring the metal in an octahedral environment (δ_I = 1.31 mm s^{-1}, $\Delta E_{Q,I}$ = 3.22 mm s^{-1} (67%) and δ_{II} = 1.34 mm s^{-1}, $\Delta E_{Q,II}$ = 2.37 mm s^{-1} (19%)), in agreement with literature data.[24] Therefore, these results suggest that at the reaction concentration (0.05 M) the iron ion adopts an octahedral environment in acetonitrile. In addition, the isomer shift is 0.1 mm s^{-1} higher than that in the solid state. The same increase has been previously measured at room temperature on powder samples between $FeCl_2{\cdot}2H_2O$ presenting the same polymeric 1D chain (δ = 1.12 mm s^{-1}) and $FeCl_2{\cdot}4H_2O$, where the ferrous ions are hexacoordinated by two chloride ions in trans positions and four water molecules (δ = 1.22 mm s^{-1}).[25] This strongly suggests that, in acetonitrile, octahedral ferrous complexes are formed with two chloride ions and four acetonitrile molecules coordinated: $[FeCl_2(S)_4]$ (**4S**) (S = $NCCH_3$), which would putatively coexist as both the trans and cis isomers. The octahedral dication $[Fe(S)_6]^{2+}$ was not detected under such conditions.[26]

The cyclic voltammetry of $[FeCl_2(S)_4]$ (**4S**; 4 mM) in acetonitrile (containing $^nBu_4NBF_4$ (0.3 M) as the supporting electrolyte) exhibited several irreversible reduction peaks (Figure 2a). One major reduction peak was observed at E^P_{R1} = −1.41 V versus the saturated calomel electrode (SCE), along with two minor reduction peaks at +0.48 and −1.92 V. On the reverse scan, a major oxidation peak was observed at −0.048 V, with minor oxidation peaks at −0.35 and +0.61 V. This result can be explained by considering the equilibrium between ionic

DOI: 10.1021/acs.organomet.7b00603
Organometallics XXXX, XXX, XXX−XXX

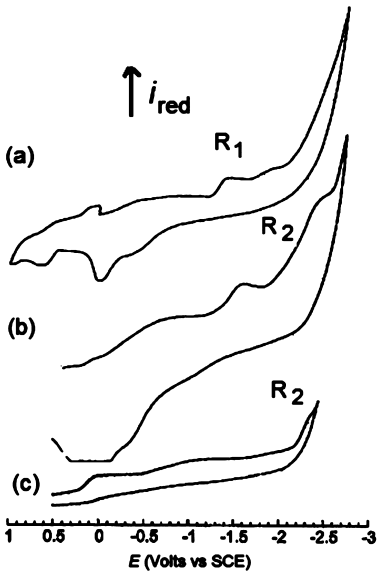

Figure 2. Cyclic voltammetry performed at a gold-disk electrode (d = 1 mm) at 22 °C in acetonitrile (S) containing $^{n}Bu_4NBF_4$ (0.3 M) as the supporting electrolyte: (a) Reduction of $[Fe^{II}Cl_2(S)_4]$ (**4S**; 4 mM) at a scan rate of 0.5 V s^{-1}; (b) $[Fe^{II}Cl_2(S)_4]$ (**4S**; 4 mM) in the presence of $NaBH_4$ (4 equiv) at a scan rate of 5 V s^{-1}; (c) reduction of isolated $[(\eta^1\text{-}H_3BH)Fe^{II}Cl(S)_4]$ (**5**; 4 mM) at a scan rate of 0.5 V s^{-1}.

species formed from $[FeCl_2(S)_4]$ (**4S**) in an acetonitrile solution (Scheme 6).[27,28] The position of the equilibrium is expected to be sensitive to the concentration and the ionic strength induced by the supporting electrolyte.

Scheme 6. Postulated Iron(II) Complexes Formed in Acetonitrile

$$[Fe^{II}Cl_2(S)_4] + n\,S \rightleftharpoons [Fe^{II}Cl_{(2-n)}(S)_{(4+n)}]^{n+} + n\,Cl^-$$

4S

$S = CH_3CN$; n = 0,1,2

Characterization of the Iron(II) Complex Formed in Situ from the Reaction of $[FeCl_2(S)_4]$ (4S) with $NaBH_4$ in Acetonitrile. The reaction of nonstabilized iron(II) and iron(III) salts such as $FeBr_2$ and $FeBr_3$ by $NaBH_4$ has been explored by several groups, and the structure of the resulting species was remarkably solvent dependent. For example, in the presence of water in diethyl ether, the reduction of $FeBr_2$ leads to the formation of noncrystalline metallic Fe^0, whereas in dry diglyme borohydride-ligated iron(II) complexes such as $[Fe(BH_4)_2(S)_n]$ (S = diglyme) are obtained, with no further reduction of the metal occurring at temperatures lower than 65 °C.[29] However, the analogous bis-borohydride complex proved to be unstable in dry diethyl ether.[30] Several well-defined iron(II) borohydride complexes supported by various (PNP) pincer ligands have been reported and characterized by X-ray diffraction.[31] In some cases, the iron center features η^1 coordination of the borohydride ligand[31] or bridging $\mu_2,\eta^1{:}\eta^1$-H_2BH_2 moieties.[31d] Some of these complexes exhibited good catalytic activities in ketone hydrogenation[31c] and methanol dehydrogenation.[32]

The reaction of $FeCl_2(S)_4$ (**4S**) with $NaBH_4$ was monitored by cyclic voltammetry. The reduction peaks of $[FeCl_2(S)_4]$ (**4S**) (Figure 2a) decreased upon addition of sodium borohydride (up to 4 equiv). At the same time a new reduction peak was observed at E^{P}_{R2} = −2.32 V (Figure 2b). The reduction peak R_2 was attributed to the formation of a new complex that has been independently synthesized and characterized to be the borohydride iron(II) complex $[(BH_4)$-$FeCl(S)4]$ (**5**) (Scheme 7) (vide infra for the characterization data).

Scheme 7. Synthesis of $[(\eta^1\text{-}H_3BH)FeCl(NCCH_3)_4]$ (5) by Reaction of $NaBH_4$ with $\{Fe(\mu\text{-}Cl)_2(NCCH_3)_2\}_n$ in Acetonitrile

$$\{Fe(\mu\text{-}Cl)_2(NCCH_3)_2\}n \xrightarrow{S = CH_3CN} [FeCl_2(S)_4]$$

solid (**4**) **4S**

$$\xrightarrow[CH_3CN,\ \Delta,\ Ar,\ 3\ h]{NaBH_4\ (0.4\ equiv)} [(\eta^1\text{-}H_3BH)FeCl(S)_4]$$

5

The isolated complex $[(\eta^1\text{-}H_3BH)FeCl(S)_4]$ (**5**) was prepared as shown in Scheme 7. Reaction of dichlorobis(acetonitrile)iron(II) (**4**) with sodium borohydride (0.4 equiv) in acetonitrile gave an orange-brown solid. This new complex (**5**) was extremely air sensitive and thermally unstable, which made its complete characterization difficult. If appropriate precautions were not taken to maintain an inert environment, a noticeable and rapid color change of the complex occurred, from dull orange-brown to bright yellow. X-ray analysis revealed that the bright yellow complex was hexakis(acetonitrile)iron(II) (μ-oxo)bis(trichloroiron(III)) ($[Fe(NCCH_3)_6][Cl_3Fe(\mu\text{-}O)FeCl_3]$).[33]

The isolated complex $[(\eta^1\text{-}H_3BH)FeCl(S)_4]$ (**5**) was characterized by cyclic voltammetry. It exhibited the same reduction peak at E^{P}_{R2} = −2.37 V (Figure 2c) as the complex generated in situ from **4S** and $NaBH_4$ (Figure 2b). The reduction peak of **5** is irreversible at low scan rate (v = 0.5 V s^{-1}, Figure 2c), indicating that the electrogenerated complex $\mathbf{5}^-$ is not stable on the time scale of the cyclic voltammetry, in contrast to $[HFe^{I}Cl(dppe)_2]^-$ ($\mathbf{3}^-$).[16] However, at a higher scan rate (v = 5 V s^{-1}, shorter time scale), the reduction peak of **5** at R_2 became partially reversible, suggesting the formation of $[(\eta^1\text{-}H_3BH)Fe^{I}Cl(NCCH_3)_4]^-$ ($\mathbf{5}^-$), which is partially stable on the time scale of this cyclic voltammogram (Figure 2b).

Monitoring the addition of two 1 equiv amounts in succession of $NaBH_4$ to $[FeCl_2(S)_4]$ (**4S**) in CD_3CN by $^{11}B\{^1H\}$ NMR in the presence of $^{n}Bu_4NBPh_4$ as an internal reference revealed that no boron-containing byproducts (such as $H_3B{\cdot}NCCH_3$ adducts) were formed. $NaBH_4$ itself could not be detected in the +500/−500 ppm range. However, free $NaBH_4$ was observed as a singlet at −41 ppm for higher $NaBH_4$ concentrations (>3 equiv/mol of iron). The reaction of $NaBH_4$ with $[FeCl_2(S)_4]$ (**4S**) in acetonitrile in the absence of any additional coligand is therefore in stark contrast with the formation of the diphosphine complex $[HFeCl(dppe)_2]$ (**3**) from $NaBH_4$ and $[FeCl_2(dppe)_2]$, which can be synthesized and isolated. In the latter case, a stable terminal hydride is indeed obtained, and hydroborane BH_3 is released in the bulk, as confirmed by the characterization of its dppe-ligated adduct by ^{31}P NMR spectroscopy.[16b] This strongly suggests that no free diamagnetic boron byproduct is released in the bulk during the reaction of $NaBH_4$ with $[FeCl_2(S)_4]$ (**4S**) in acetonitrile and that at least one borohydride anion could act as a ligand to a paramagnetic NMR-silent species. This hypothesis is consistent with the work of Klabunde mentioned earlier, who reported that $FeBr_2$ reacted with an excess of $NaBH_4$ in diglyme

DOI: 10.1021/acs.organomet.7b00603
Organometallics XXXX, XXX, XXX−XXX

Table 2. Parameters Determined from the Simulations of the Mössbauer Spectra Shown in Figure 1[a]

addition of $NaBH_4$	dite	volor	δ (mm s^{-1})	ΔE_Q (mm s^{-1})	Γ (mm s^{-1})[b]	rel area (%)
no[c]	I	dark green	1.31	3.22	0.37	67
	II	light green	1.34	2.37	0.50	19
	III	orange	0.30	0.70	0.60	13
yes[d]	IV	dark blue	1.25	2.90	−0.35	43
	V	light blue	1.18	2.23	0.53	34
	VI	red	0.46	0.74	0.51	24

[a]Uncertainties are ±0.03 mm s^{-1} on the isomer shift δ, ±0.05 mm s^{-1} on the quadrupole splitting ΔE_Q, and ±2% on the relative area. [b]The Lorentzian line presents a full width at half-maximum (fwhm) denoted as Γ. A negative value indicates a Voigt line shape, which is the convolution of a 0.19 mm s^{-1} fwhm Lorentzian line with a Gaussian whose fwhm is the absolute value of Γ. [c]Mössbauer spectrum shown in Figure 1a. [d]Mössbauer spectrum shown in Figure 1b.

to give diglyme-stabilized bis-borohydride complexes such as $[Fe(BH_4)_2(S)_n]$ (S = diglyme).[29] Moreover, high-resolution ESI mass spectrometry revealed that, after ionization, $[(\eta^1\text{-}H_3BH)FeCl(S)_4]$ (**5**) exhibited the same fragment ion $[FeCl(S)_2]^+$ as **4**, resulting from the loss of a borohydride fragment and two acetonitrile ligands (calcd 172.95634, found 172.95650).[34] Taken together, these results suggest that, in the presence of a moderate excess of $NaBH_4$ in acetonitrile solution, $[FeCl_2(S)_4]$ (**4S**) reacts to form an iron(II) borohydride complex such as $[(\eta^1\text{-}H_3BH)FeCl(S)_4]$ (**5**) by substitution of a single chloride ligand.

The IR spectrum of $[(\eta^1\text{-}H_3BH)FeCl(S)_n]$ (**5**, solid phase, Nujol) confirmed the η^1 coordination mode of the borohydride ligand. Well-defined stretches characteristic of a transition-metal-ligated η^1-borohydride anion were observed at 2429, 2390, and 2352 cm^{-1} (ν_{BH3}) and 2042 cm^{-1} (ν_{Fe-H-B}).[31a] The BH_3 deformation band could not be assigned precisely due to the presence of other signals in the 900−1100 cm^{-1} area (see the Supporting Information). No signal characteristic of a terminal Fe−H bond vibration in the 1800−2000 cm^{-1} range (usual range for the M−H bond vibration) could be detected, thus excluding the formation of a terminal iron hydride. These data are in good agreement with previous reports for (η^1-borohydrido)iron(II) species by Koehne[31d] and Field.[31b] However, it should be noted that almost all of the reported iron(II) borohydride or terminal hydride complexes accommodate a low-spin configuration.

More structural insights into the nature of this borohydride species under solvation conditions were gained by Mössbauer spectroscopy on frozen solutions, starting from ^{57}Fe-enriched complexes. Figure 1b shows the zero-field Mössbauer spectrum recorded at 80 K on a 0.05 M acetonitrile solution of $^{57}FeCl_2$ after the addition of excess $NaBH_4$. The addition of 18 or 53 equiv of $NaBH_4$ leads to identical spectra. Accordingly, only the spectrum with 53 equiv is shown. The lines are quite broad; however, this spectrum significantly differs from that recorded for $[FeCl_2(S)_4]$ (**4S**) (Figure 1a). A reduced separation of the two more intense lines, now at 0 and 2.8 mm s^{-1} versus −0.3 and 3.0 mm s^{-1} for **4S**, is observed. In addition, a new line is detected at 0.7 mm s^{-1}. The slight shift of the high-velocity pattern indicates that the starting Fe^{II} species has reacted with $NaBH_4$ and that new high-spin Fe^{II} species are generated.

The spectrum shown in Figure 1b was then simulated. In order to reproduce the asymmetric profile of the high-velocity line, three doublets must be considered. The simulation is shown in Figure 1b, and the parameters are given in Table 2. Two doublets (IV and V) present isomeric shift values lying between 1.1 and 1.3 mm s^{-1} (δ_{IV} = 1.25 mm s^{-1}, $\Delta E_{Q,IV}$ = 2.90 mm s^{-1} (43%) and δ_V = 1.18 mm s^{-1}, $\Delta E_{Q,V}$ = 2.23 mm s^{-1} (34%)), which correspond to high-spin ferrous ions accommodating an octahedral environment, these sites accounting for 77% of the total iron content. The isomeric shift value associated with the third doublet (VI) is much lower (δ_{IV} = 0.46 mm s^{-1}), which renders this doublet more difficult to assign. Because borohydride was added in great excess, a reasonable hypothesis is that it is associated with a reduced form of iron. This is in agreement with the cyclic voltammogram recorded after addition of 50 equiv of $NaBH_4$ (see the Supporting Information). A broad oxidation peak is detected at E^p_{O1} = +0.2 V vs SCE, indicating the chemical reduction of Fe^{II} to metallic Fe^0. The same peak is also observed on the reverse scan in Figure 2a and corresponds to the oxidation of the electrogenerated reduced species adsorbed at the electrode and formed upon electroreduction of $[FeCl_2(S)_4]$ (**4S**).

DFT calculations were performed to gain further insights into the high-spin ferrous species **5** generated by the reaction of $NaBH_4$ with $[FeCl_2(S)_4]$ (**4S**). Alternative structures were also computed for comparison (Scheme 8). Because the isomer shifts of the doublets labeled IV and V (Table 2) are significantly lower than those of the starting species (doublets I and II, Table 2), it is reasonable to postulate the substitution of one ligand by a stronger σ donor: namely, borohydride or hydride. Calculations were performed on several model complexes (see the Supporting Information). The negatively

Scheme 8. Distribution of (a) Mono- and (b) Bis-Borohydrido Fe^{II} Species Obtained by Reaction of Excess $NaBH_4$ with $[FeCl_2(S)_4]$(4S) in Acetonitrile

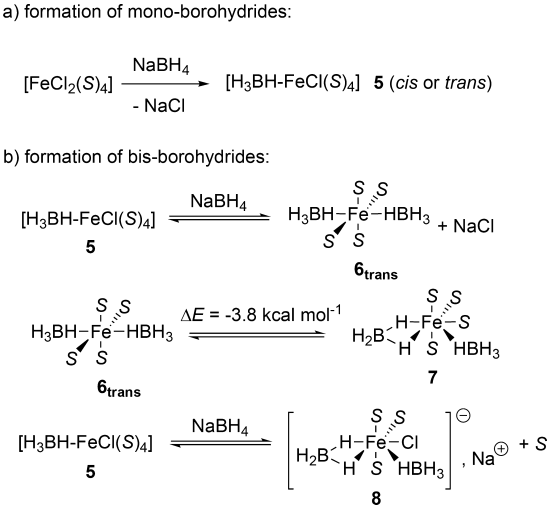

DOI: 10.1021/acs.organomet.7b00603
Organometallics XXXX, XXX, XXX−XXX

charged ligands (Cl^-, BH_4^-, H^-) may be in the cis or trans positions, and the borohydrido ligand may coordinate in the η^1 or κ^2 mode. Since $NaBH_4$ is present in great excess, the coordination of two borohydride ligands was also considered. A selection of calculated isomer shift values is given in Table 3.

Table 3. Calculated Isomer Shifts (δ) for Several Relevant High-Spin Fe^{II} Borohydrides[a]

label	complex	ρ_0(calcd) (e a_0^{-3})	δ(calcd) (mm s^{-1})
$\mathbf{5}_{trans}$	*trans*-[(η^1-H_3BH)FeCl($NCCH_3$)$_4$]	11816.89	1.20
$\mathbf{5}_{cis}$	*cis*-[(η^1-H_3BH)FeCl($NCCH_3$)$_4$]	11816.85	1.21
$\mathbf{6}_{trans}$	*trans*-[(η^1-H_3BH)$_2$Fe($NCCH_3$)$_4$]	11817.08	1.13
7	[(κ^2(*H*,*H*)-H_2BH_2)(η^1-H_3BH)Fe($NCCH_3$)$_4$]	11816.76	1.27
8	[(κ^2(*H*,*H*)-H_2BH_2)(η^1-H_3BH)FeCl($NCCH_3$)$_3$]$^-$	11816.69	1.27

[a]The calculated isomer shift values are deduced from the correlation curve established in the Supporting Information.

Solvated complex **5** was tentatively assigned as the borohydrido complex [(η^1-H_3BH)FeCl($NCCH_3$)$_4$] in the solid phase (Scheme 7). Simulations of the Mössbauer parameters of the trans and cis isomers of [(η^1-H_3BH)FeCl($NCCH_3$)$_4$] (**5**) were performed (Scheme 8a). Complexes $\mathbf{5}_{trans}$ and $\mathbf{5}_{cis}$ were found to be almost isoenergetic ($\Delta E \approx 1$ kcal mol^{-1}), with similar nuclear parameters (δ = 1.20 mm s^{-1} ($\mathbf{5}_{trans}$); δ = 1.21 mm s^{-1} ($\mathbf{5}_{cis}$); Table 3). It was found that the parent hydrides [HFeCl($NCCH_3$)$_4$] led to smaller values of the isomer shift (ca. 1.1 mm s^{-1}), in agreement with H^- having stronger σ donating properties in comparison BH_4^- (see the Supporting Information).

Therefore, computed parameters of monoborohydrido complexes $\mathbf{5}_{trans}$ and $\mathbf{5}_{cis}$ (Table 3, and Scheme 8a) reproduce the simulation of doublet V in the experimental spectrum well (Figure 1b and Table 2). Due to the high borohydride to iron ratio (18 or 53 equiv) in the Mössbauer experiments, bis-borohydrido complexes can also be obtained. Complexes [(η^1-H_3BH)$_2$Fe($NCCH_3$)$_4$] (**6**) can be formed by substitution of the remaining chloride anion of **5** by a second borohydride. DFT calculations show that **6** evolve(s) toward the more stable complex **7** [(κ^2(*H*,*H*)-H_2BH_2)(η^1-H_3BH)Fe($NCCH_3$)$_4$] (ΔE = −3.8 kcal mol^{-1}, Scheme 8b). In complex **7**, the steric pressure in the meridional plane containing five ligands leads to longer metal−ligand bonds and therefore to an electronic density at the ^{57}Fe nucleus smaller than that for the octahedral species $\mathbf{5}_{trans}$ and $\mathbf{5}_{cis}$. Consequently, the corresponding isomer shift is higher (δ = 1.27 mm s^{-1}, **7**; Table 3). Analogously, [(κ^2(*H*,*H*)-H_2BH_2)(η^1-H_3BH)FeCl($NCCH_3$)$_3$]$^-$ (**8**), formed from **5** via substitution of an acetonitrile molecule by BH_4^-, was computed (Scheme 8b). Complex **8** gave a similarly high computed isomer shift (δ = 1.27 mm s^{-1}, **8**; Table 3) to **7**. Therefore, the doublet IV in the spectrum (Figure 1b and Table 2) can be explained by the formation of sterically constrained bis-borohydrido species such as **7** and **8**, which exhibit isomer shifts higher than those of **5**.

Computation of mono and bis iron(II) borohydride nuclear parameters can explain the general trend observed in the Mössbauer experimental spectrum.[35] Moreover, the formation of bis-borohydrido species can explain the fast formation of reduced oxidation states leading to the observation of the doublet VI in Figure 1b. However, due to the broadness of the experimental signals, it can be anticipated that several structurally similar isomers (or other species with similar nuclear parameters) coexist in solution.

Iron(II) Hydride versus Iron(II) Borohydride Complexes. As stated in the previous section, there is a major difference in the electronic properties of the Fe^{II}−H bond in the well-defined diphosphine-ligated complex [HFeCl(dppe)$_2$] (**3**) and in borohydride acetonitrile-ligated complexes such as [(η^1-H_3BH)FeCl($NCCH_3$)$_4$] (**5**). The former is a low-spin Fe^{II} terminal hydride, whereas the latter is a high-spin Fe^{II} borohydride. This difference is well reflected by DFT calculations. The computation of the enthalpy of formation of the dppe-stabilized borohydride *trans*-[(η^1-H_3BH)FeCl(dppe)$_2$] ($\mathbf{3'}_{trans}$) from *trans*-[HFeCl(dppe)$_2$] ($\mathbf{3}_{trans}$) and the $H_3B{\cdot}NCCH_3$ adduct clearly shows that the terminal hydride **3** is more stable than the corresponding borohydride $\mathbf{3'}_{trans}$ (ΔE = 10.7 kcal mol^{-1}; Scheme 9a). This equilibrium is the opposite

Scheme 9. DFT-Computed Equilibria between Hydrides and Borohydrides for Complexes (a) 3 and 3′ and (b) 5 and 5′[a]

a) [HFeCl(dppe)$_2$] + $H_3B{\bullet}S$ ⇌ [η^1−H_3BHFeCl(dppe)$_2$] + S
3 (0.0) **3'** (10.7)

b) [η^1−H_3BHFeCl(S)$_4$] + S ⇌ [HFeCl(S)$_4$] + $H_3B{\bullet}S$
5 (0.0) **5'** (16.2)

[a]All complexes were computed as trans isomers. Values in parentheses stand for the energies in kcal mol^{-1}.

for the acetonitrile-ligated system, which is shown to be far more stabilized in the borohydride form, with *trans*-[(η^1-H_3BH)FeCl($NCCH_3$)$_4$] ($\mathbf{5}_{trans}$) stabilized by ca. ΔE = 16.2 kcal mol^{-1} with respect to the corresponding hydride *trans*-[HFeCl($NCCH_3$)$_4$] ($\mathbf{5'}_{trans}$; Scheme 9b).

An analysis of the electronic population of *trans*-[HFeCl(dppe)$_2$] ($\mathbf{3}_{trans}$) by natural bond orbital (NBO) theory shows that there is a strong delocalization of the σ(Fe−H) molecular orbital into the antibonding σ^*(Fe−P) MOs. The analysis is drastically different for the acetonitrile-ligated complex *trans*-[HFeCl($NCCH_3$)$_4$] ($\mathbf{5'}_{trans}$), where no significant delocalization of the σ(Fe−H) molecular orbital into the acetonitrile ligands is observed. Consistent with this observation, all of the spin density is located on the iron center in *trans*-[HFeCl($NCCH_3$)$_4$] ($\mathbf{5'}_{trans}$) (computed Mulliken spin density on iron 4.00, which is the expected theoretical value for a high-spin Fe^{II} ion), and the iron-ligated acetonitrile ligands remain mostly neutral (average computed NBO charge for each acetonitrile ligand q = +0.04 |e|), showing that no charge transfer occurs from the Fe^{II}−H moiety.

Chlorotetrakis(acetonitrile)iron(II) Borohydride Complex 5 as Precatalyst for Reactions of Unsaturated Haloacetals. [(η^1-H_3BH)Fe^{II}Cl($NCCH_3$)$_4$] (**5**) was tested as a suitable precatalyst for reaction with haloacetals (**1**), as shown in Scheme 10.

Indeed, [(η^1-H_3BH)Fe^{II}Cl($NCCH_3$)$_4$] (**5**) catalyzed the reaction of both iodoacetal ($\mathbf{1}_I$) and bromoacetal ($\mathbf{1}_{Br}$) substrates in the presence of 1.0 equiv of $NaBH_4$ (Table 4), in contrast to [HFeCl(dppe)$_2$] (**3**), which only mediated the reaction of iodoacetal ($\mathbf{1}_I$). Complete conversion and good yields were obtained for iodoacetals $\mathbf{1}_I$ and $\mathbf{1}_{InPr}$ (entries 1 and 3, Table 4). In the case of $\mathbf{1}_{IMe}$ a moderate yield (46%) of the bicyclic product ($\mathbf{2}_{diMe}$) was obtained along with 19% recovery of the starting material (entry 5). The unsubstituted bromoacetal ($\mathbf{1}_{Br}$) was completely consumed in the reaction, and 57% of bicyclic product ($\mathbf{2}_H$) was obtained (entry 2, Table

DOI: 10.1021/acs.organomet.7b00603
Organometallics XXXX, XXX, XXX−XXX

Scheme 10. Reaction of Haloacetals 1 in the Presence of $[(\eta^1\text{-}H_3BH)Fe^{II}Cl(NCCH_3)_4]$ (5) and $NaBH_4$

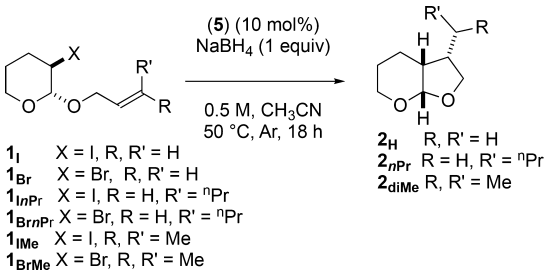

Table 4. Reactivity of Haloacetals 1 in the Presence of $[(\eta^1\text{-}H_3BH)Fe^{II}Cl(NCCH_3)_4]$ (5) (10 mol %) and Sodium Borohydride (1 equiv)[a]

entry	substrate	yield of 2 (%) (recovered 1 (%)) [dr]
1	$\mathbf{1_I}$	77 (0) [88:12]
2	$\mathbf{1_{Br}}$	57 (0) [86:14]
3	$\mathbf{1_{InPr}}$	70 (0) [82:18]
4	$\mathbf{1_{BrnPr}}$	38 (38) [81:19]
5	$\mathbf{1_{IMe}}$	46 (19) [66:34]
6	$\mathbf{1_{BrMe}}$	23 (55) [65:35]

[a]Reaction conditions: 1 (1.0 mmol, 0.5 M in CH_3CN), $[(\eta_1\text{-}H_3BH)Fe^{II}Cl(NCCH_3)_4]$ (5) (10 mol %), $NaBH_4$ (1 equiv), 50 °C, 18 h.

4). Substituted bromoacetals ($\mathbf{1_{BrnPr}}$ and $\mathbf{1_{BrMe}}$) were reactive, albeit with incomplete conversion, giving the bicyclic products in 38% yield ($\mathbf{2_{nPr}}$, entry 4, Table 4) and 23% yield ($\mathbf{2_{diMe}}$, entry 6), respectively.

Mechanistic Studies: Exploring Reactivity Differences. This raised an important question about the ability of the iron(II) monohydride or borohydride complexes, ligated by either phosphorus ligands (3) or acetonitrile ligands (5), to act as precatalysts for the reaction of bromoacetal ($\mathbf{1_{Br}}$).

Cyclic voltammetry had been used to evidence the catalytic turnover of the active iron(I) anionic hydride catalyst $[HFe^{I}Cl(dppe)_2]^-$ ($\mathbf{3^-}$) in the presence of iodoacetal ($\mathbf{1_I}$).[16] Thus, the catalytic activity of $[(\eta^1\text{-}H_3BH)Fe^{I}Cl(NCCH_3)_4]^-$ ($\mathbf{5^-}$) in the presence of haloacetals ($\mathbf{1_I}$ and $\mathbf{1_{Br}}$) was also tested by electrochemistry. The reduction potential of iodoacetal ($\mathbf{1_I}$) in acetonitrile was measured at $E^{P}_{red} = -2.5$ V vs. SCE at a scan rate of 0.5 V s^{-1}. In contrast, the reduction potential of bromoacetal ($\mathbf{1_{Br}}$) could not be measured, as the substrate was not reduced before the solvent ($E^{P}_{red} = -2.7$ V vs. SCE). As shown in Figure 3a, in the presence of iodoacetal ($\mathbf{1_I}$), the reduction peak R_2 of $[(\eta^1\text{-}H_3BH)Fe^{II}Cl(NCCH_3)_4]$ (5) increases with each aliquot of substrate (0–10 equiv, Figure 3a). Therefore, the anionic species $[(\eta^1\text{-}H_3BH)Fe^{I}Cl(NCCH_3)_4]^-$ ($\mathbf{5^-}$) (generated by electrochemical reduction of $[(\eta^1\text{-}H_3BH)Fe^{II}Cl(NCCH_3)_4]$ (5)) activates iodoacetal ($\mathbf{1_I}$) by electron transfer. This in turn regenerates $[(\eta^1\text{-}H_3BH)Fe^{II}Cl(NCCH_3)_4]$ (5), and a catalytic current was observed. This reveals that the interaction of $[(\eta^1\text{-}H_3BH)Fe^{I}Cl(NCCH_3)_4]^-$ ($\mathbf{5^-}$) with $\mathbf{1_I}$ is faster than its decomposition on the time scale of cyclic voltammetry.

The procedure was repeated in the presence of bromoacetal ($\mathbf{1_{Br}}$). A noticeable catalytic effect in the presence of $\mathbf{1_{Br}}$ was observed, as shown in Figure 3b (0–12 equiv). This result provides strong evidence that the acetonitrile ligated $[(\eta^1\text{-}H_3BH)Fe^{II}Cl(NCCH_3)_4]$ (5) furnishes the catalytic species $[(\eta^1\text{-}H_3BH)Fe^{I}Cl(NCCH_3)_4]^-$ ($\mathbf{5^-}$) able to activate both $\mathbf{1_I}$ and $\mathbf{1_{Br}}$. The turnover was lower for $\mathbf{1_{Br}}$ than for $\mathbf{1_I}$ (compare the catalytic currents in parts b and c of Figures 3, respectively).

No catalytic current at R_3 was observed when $[HFeCl(dppe)_2]$ (3) was reduced in the presence of increasing amount of $\mathbf{1_{Br}}$ (1–6 equiv, Figure 3c), in contrast to the case for $[(\eta^1\text{-}H_3BH)Fe^{II}Cl(NCCH_3)_4]$ (5) (Figure 3b). Therefore, anionic $[(\eta^1\text{-}H_3BH)Fe^{I}Cl(NCCH_3)_4]^-$ ($\mathbf{5^-}$) promotes the reduction of $\mathbf{1_{Br}}$ in contrast to $[HFe^{I}Cl(dppe)_2]^-$ ($\mathbf{3^-}$), in agreement with the experimental observations. This shows that the ligand structure (hydride versus borohydride) strongly affects the reactivity of the anionic iron(I) complex with $\mathbf{1_{Br}}$.

These results have interesting mechanistic implications to explain the higher reactivity of bromoacetal ($\mathbf{1_{Br}}$) in the presence of $[(\eta^1\text{-}H_3BH)Fe^{II}Cl(NCCH_3)_4]$ (5) versus $[HFe^{II}Cl(dppe)_2]$ (3).

The rate of electron transfer of $[(\eta^1\text{-}H_3BH)Fe^{I}Cl(NCCH_3)_4]^-$ ($\mathbf{5^-}$) or $[HFe^{I}Cl(dppe)_2]^-$ ($\mathbf{3^-}$) to haloacetals is controlled by the potential gap (ΔE) between the reduction potential of the haloacetals and the oxidation potential of the anionic iron(I) (boro)hydride complexes. This potential gap is

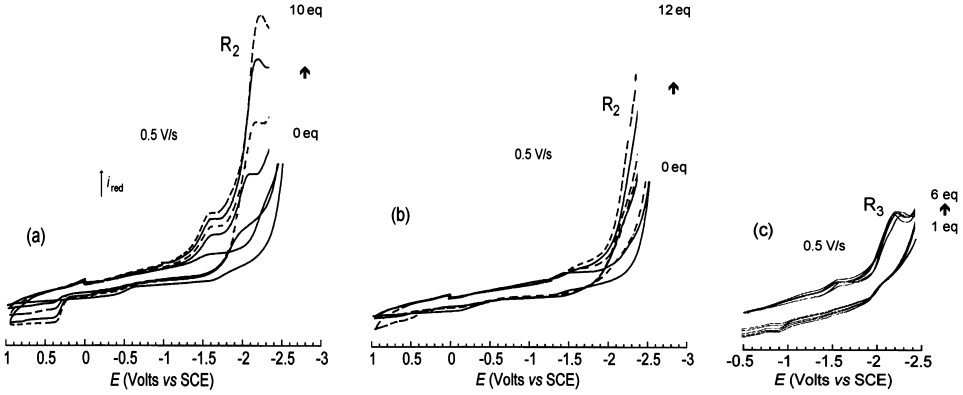

Figure 3. Cyclic voltammetry performed at a gold-disk electrode (d = 1 mm) at 22 °C in acetonitrile containing $^nBu_4NBF_4$ (0.3 M) as the supporting electrolyte at a scan rate of 0.5 V s^{-1}: (a) reduction of $[(\eta^1\text{-}H_3BH)Fe^{II}Cl(NCCH_3)_4]$ (4 mM) in the presence of increasing amounts of $\mathbf{1_I}$ (0 and 4 equiv, solid lines; 6 equiv, dashed line; 8 equiv, solid line; 10 equiv, dashed line); (b) reduction of $[(\eta^1\text{-}H_3BH)Fe^{II}Cl(NCCH_3)_4]$ (4 mM) in the presence of increasing amounts of $\mathbf{1_{Br}}$ (0 and 8 equiv, solid lines; 4 and 12 equiv, dashed lines); (c) reduction of $[HFe^{II}Cl(dppe)_2]$ (4 mM) in the presence of increasing amounts of $\mathbf{1_{Br}}$ (1–6 equiv, solid lines).

DOI: 10.1021/acs.organomet.7b00603
Organometallics XXXX, XXX, XXX–XXX

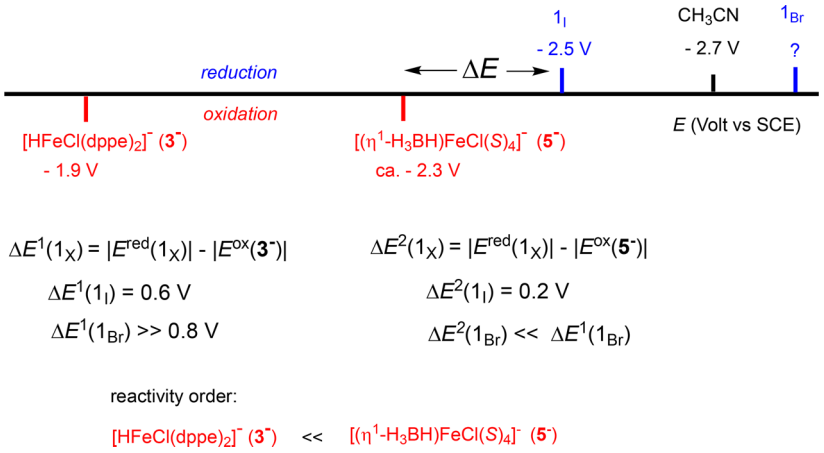

Figure 4. Cyclic voltammetry data used to explain the difference in reactivity of anionic complexes $\mathbf{3}^-$ and $\mathbf{5}^-$ with iodo- and bromoacetals ($\mathbf{1}_X$) (X = I, Br).

crucial to the outcome of the reaction: indeed, the lower the potential gap, the faster the reaction.[36]

As stated earlier, $\mathbf{1}_I$ is more easily reduced than $\mathbf{1}_{Br}$ at −2.5 V and more negative than −2.7 V, respectively (Figure 4). $[HFe^ICl(dppe)_2]^-$ ($\mathbf{3}^-$) is less easily oxidized (−1.9 V)[16a] than $[(\eta^1\text{-}H_3BH)Fe^ICl(NCCH_3)_4]^-$ ($\mathbf{5}^-$) (estimated to be ca. −2.3 V) (Figure 4).

$[HFe^ICl(dppe)_2]^-$ ($\mathbf{3}^-$) reacts with $\mathbf{1}_I$ because of the low potential gap, $\Delta E^1(\mathbf{1}_I)$ = 0.6 V, which permits a fast reaction (Figure 4). The reaction with $\mathbf{1}_I$ is even faster with $[(\eta^1\text{-}H_3BH)Fe^ICl(S)_4]^-$ ($\mathbf{5}^-$) because the potential gap $\Delta E^2(\mathbf{1}_I)$ is even lower (0.2 V) (Figure 4).

The potential gap $\Delta E^1(\mathbf{1}_{Br})$ between $[HFe^ICl(dppe)_2]^-$ ($\mathbf{3}^-$) and $\mathbf{1}_{Br}$ is larger than 0.8 V. This explains why the catalytic reaction does not proceed when $[HFe^{II}Cl(dppe)_2]$ ($\mathbf{3}$) is used as the precatalyst. The potential gap $\Delta E^2(\mathbf{1}_{Br})$ between $\mathbf{5}^-$ and $\mathbf{1}_{Br}$ is smaller than $\Delta E^1(\mathbf{1}_{Br})$ ($\Delta E^2(\mathbf{1}_{Br}) < \Delta E^1(\mathbf{1}_{Br})$, Figure 4), and therefore $[(\eta^1\text{-}H_3BH)Fe^ICl(S)_4]^-$ ($\mathbf{5}^-$) can activate $\mathbf{1}_{Br}$ and the catalytic reaction proceeds. In conclusion, the acetonitrile ligand renders the corresponding catalytically active species ($\mathbf{5}^-$) far more active than the phosphine ligand ($\mathbf{3}^-$). This clearly demonstrates the importance of the ligand in determining the outcome of the catalytic reaction.

Mechanism. The results of the catalytic reactions and subsequent mechanistic investigation performed on $[(\eta^1\text{-}H_3BH)Fe^{II}Cl(NCCH_3)_4]$ ($\mathbf{5}$) provides evidence for the active catalyst, the anionic iron(I) borohydride species $[(\eta^1\text{-}H_3BH)Fe^ICl(NCCH_3)_4]^-$ ($\mathbf{5}^-$) (Figure 5). The latter is formed from the iron(II) borohydride precatalyst $\mathbf{5}$, either by electrochemical means or by $NaBH_4$. Activation of RX ($\mathbf{1}_X$, X = I, Br) by $\mathbf{5}^-$ via electron transfer generates the radical $R^\bullet$ involved in the cyclization process. Hydrogen atom transfer to form the final cyclized product R′H occurs either directly from BH_4^- or from $[(\eta^1\text{-}H_3BH)Fe^{II}Cl(NCCH_3)_4]$ ($\mathbf{5}$) (vide infra for the computational studies that model the final step).[37]

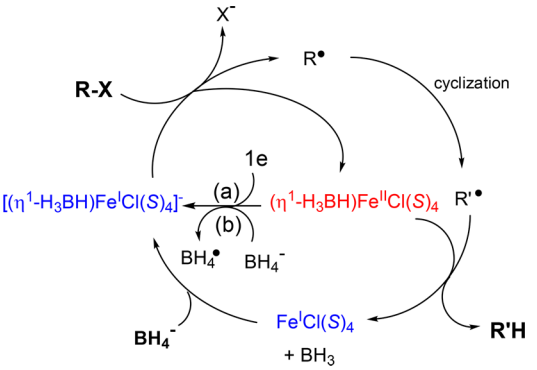

Figure 5. Mechanistic role of the active anionic iron(I) borohydride complex (blue) generated either (a) by electrochemical reduction or (b) by reduction by $NaBH_4$ of the iron(II) borohydride complex (red).

CONCLUSIONS

In conclusion it is established that the structure and reactivity of the active iron catalyst in the cyclization of unsaturated iodo- and bromoacetals is directly related to the ligand environment (acetonitrile versus dppe). The iron(II) borohydride $[(\eta^1\text{-}H_3BH)FeCl(NCCH_3)_4]$ ($\mathbf{5}$) has been synthesized, and its catalytic and redox properties have been compared to those of the reported iron(II) hydride $[HFeCl(dppe)_2]$ ($\mathbf{3}$).[16] As observed by cyclic voltammetry, the anionic iron(I) complex $[(\eta^1\text{-}H_3BH)FeCl(NCCH_3)_4]^-$ ($\mathbf{5}^-$) is able to activate both iodo- and bromoacetals, in contrast to $[HFeCl(dppe)_2]^-$ ($\mathbf{3}^-$), which can only activate the iodoacetal. This result is in agreement with the synthetic reactions in which the precatalyst $[(\eta^1\text{-}H_3BH)FeCl(NCCH_3)_4]$ ($\mathbf{5}$) mediates the cyclization of the bromoacetal, while $[HFeCl(dppe)_2]$ ($\mathbf{3}$) cannot. The potential gap between the reduction potential of the haloacetal and the oxidation potential of the anionic hydrido ($\mathbf{3}^-$) or borohydrido ($\mathbf{5}^-$) iron(I) complex is crucial for the reaction outcome. When the potential gap is too large, the SET is too slow and the catalytic reaction does not occur. This rationalizes the role of the ligand which is responsible for the formation of either hydrido iron(II)/iron(I) complexes (ligand dppe) or borohydrido iron(II)/iron(I) complexes (ligand acetonitrile), which possess different redox properties.

These findings emphasize new perspectives to be considered in the design of new radical mediators. The fine tailoring of the ligand on the metal center is key to the success of such an approach. Work is underway to use this understanding to identify potential ligand candidates and validate them as efficient precatalysts for a wider range of radical reactions.

EXPERIMENTAL SECTION

General Considerations. All reactions were carried out in oven-dried glassware under an argon atmosphere using standard Schlenk

DOI: 10.1021/acs.organomet.7b00603
Organometallics XXXX, XXX, XXX−XXX

techniques. Reaction solvents (acetonitrile and dichloromethane) were degassed with argon and dried using a PureSolv Micro Solvent Purification System (Innovative Technology) by percolation through a column packed with neutral alumina under a positive pressure of argon. Other solvents were dried and distilled prior to use by literature methods. All solvents were further degassed via freeze/pump/thaw cycles with argon prior to use. Column chromatography was performed using Merck Geduran SI 60 Å silica gel (35−70 μm).[2] Purification was performed using Sigma-Aldrich 58 Å neutral alumina (Brockman I, activated) as required. All substrates were filtered through neutral alumina prior to use. Iron(II) dichloride (anhydrous beads, ~10 mesh, 99.99%) and sodium borohydride (99.99%) were purchased from Sigma-Aldrich. These reagents were stored in the glovebox and used as received. NMR spectra were recorded on a Bruker AV400 or Avance III spectrometer fitted with either a QNP or BBFO probe and calibrated using undeuterated acetonitrile (δ_H 1.94 ppm and δ_C 118.26) or chloroform (δ_H 7.26 ppm and δ_C 77.16 ppm) as internal references. High-resolution ESI mass spectra were recorded using a FT-ICR mass spectrometer (7 T hybrid FTICR Solarix spectrometer, Bruker Daltonik GmbH) combined with an ion funnel geometry to transfer the formed ions. Cyclic voltammetry (CV) was performed with a laboratory-made potentiostat and a PAR Model 175 waveform generator. The working electrode was a steady gold disk (d = 1 mm), the counter electrode a platinum wire (ca. 0.2 cm^2 apparent area), and the reference a saturated calomel electrode. Cyclic voltammograms were recorded with a Nicolet 3091 digital oscilloscope. All experiments were carried out under argon.

Typical Procedure for the Synthesis of Iron Complexes. *trans-Hydridochlorobis{1,2-bis(diphenylphosphino)ethane}iron(II), trans-[HFeCl(dppe)$_2$] (**3**)..*[17,38] Iron(II) dichloride (160 mg, 1.3 mmol) and bis(diphenylphosphino)ethane (1.00 g, 2.5 mmol) were placed in a Schlenk flask in the glovebox, and then ethanol (15 mL) was added under argon. The mixture was stirred vigorously for 10 min and then heated to 50 °C. Sodium borohydride (29 mg, 0.76 mmol) was placed in a separate Schlenk tube in the glovebox, ethanol (12 mL) was added under argon, and the solution was stirred for 10 min. The sodium borohydride solution was added over 15 min to the iron mixture under a counter current of argon. After 2 h the reaction mixture had turned bright red-purple with both red and white precipitates. The reaction mixture was filtered, and the filtrate was washed with distilled water (dried and degassed, 2 mL) and ethanol (dried and degassed, 2 mL) and then dried under vacuum. Benzene (dried and degassed, 20 mL) was added (not all precipitate dissolved) and the solution was filtered under argon. The solvent was removed to give a red-purple solid (550 mg, 49%), which was dried under vacuum. The complex was stable in the glovebox for more than 6 months. The title compound had spectral properties identical with those previously reported.

*Dichlorobis(acetonitrile)iron(II) (**4**).*[39] Iron(II) chloride (1.00 g, 7.9 mmol) was placed in a Schlenk tube in the glovebox. Acetonitrile (5 mL) was added under argon, and the reaction mixture was heated to reflux for 3 h. The reaction mixture was cooled to room temperature, resulting in the precipitation of a solid. The solvent was removed under argon, and the solid was washed with toluene (dried and degassed, 2 mL) and hexane (dried and degassed, 2 mL) and then dried under vacuum to give colorless fine crystals (1.40 g, 85%). The complex was stable in the glovebox for more than 6 months. Crystals suitable for single-crystal X-ray crystallography were obtained directly from the mother liquor and corresponded to the data previously reported.

*Chlorotetrakis(acetonitrile)iron(II) Borohydride (**5**).* Dichlorobis(acetonitrile)iron(II) (**4**; 360 mg, 1.7 mmol) was placed in a Schlenk flask in the glovebox, acetonitrile (15 mL) was added under argon, and the mixture was stirred for 10 min. Sodium borohydride (30 mg, 0.76 mmol) was placed in a separate Schlenk tube in the glovebox, acetonitrile (12 mL) was added under argon, and the solution was stirred vigorously for 10 min. The sodium borohydride solution was added over 15 min to the iron mixture under a counter current of argon. After 3 h the reaction mixture had turned dark orange with some precipitate observed. The reaction mixture was filtered under argon, the filtrate was concentrate,d and the resulting orange-brown solid (255 mg, 56%) was dried under vacuum and stored under argon.

Typical Procedure for the Synthesis of Haloacetal Substrates. A mixture of *N*-halosuccinimide (76 mmol) and alcohol (74 mmol) in dichloromethane (40 mL) was cooled to −10 °C, and then 3,4-dihydro-2*H*-pyran (6.8 mL, 75 mmol) was added dropwise under argon. The reaction mixture was warmed to room temperature over 3 h and stirred at this temperature overnight. The reaction mixture was diluted with dichloromethane (40 mL) and washed with saturated sodium thiosulfate (3 × 20 mL). The combined aqueous phase was extracted with dichloromethane (3 × 20 mL), the combined organic phase was washed with brine (20 mL) and dried (phase separation paper), and the solvent was removed in vacuo. The residue was purified by column chromatography (20% diethyl ether/80% pentane) to afford the title compound. The product was filtered through neutral alumina prior to use.

Typical Procedure for Cyclization of Haloacetal Substrates. The iron complex (0.1 mmol) and reducing agent were placed in a screw-cap tube in the glovebox (the tube was capped with a Suba-Seal). Acetonitrile (1.5 mL) was added under argon, and the mixture was stirred for ca. 15 min at room temperature. A solution of haloacetal (1.0 mmol) in acetonitrile (0.5 mL) was added under argon, the Suba-Seal was replaced by a screw cap, and the reaction mixture was heated to 50 °C overnight. The reaction mixture was cooled to room temperature and quenched with water (20 mL), and the aqueous phase was extracted with dichloromethane (3 × 20 mL). The combined organic phase was washed with brine (30 mL) and dried (phase separation paper), and the solvent was removed in vacuo. The residue was purified by flash chromatography (5−20% diethyl ether/pentane).

Electrochemical Analyses. Cyclic voltammetry (CV) was performed in a three-electrode cell connected to a Schlenk line (under argon) at room temperature with a laboratory-made potentiostat and a PAR Model 175 waveform generator. The working electrode was a steady gold disk (d = 1 mm) and the counter electrode a platinum wire (ca. 0.2 cm^2 apparent area). The reference was a saturated calomel electrode (SCE) separated from the solution by a bridge filled with tetrabutylammonium tetrafluoroborate in acetonitrile solution (0.3 M, 2 mL). The same solution (0.3 M, 12 mL) was used as the solvent in the electrochemical cell for all CV experiments reported herein. Cyclic voltammograms were recorded with a Nicolet 3091 digital oscilloscope. All experiments were carried out under argon.

General Procedure A: Determination of Redox Potentials. Substrate (0.048 mmol, 4 mM) was placed in the electrochemical cell containing a solution of tetrabutylammonium tetrafluoroborate in acetonitrile (0.3 M, 12 mL). The CV was performed immediately after mixing, at a scan rate of 0.5 V s^{-1}.

General Procedure B: Electrochemical Reduction of Iron Complexes in the Presence of Sodium Borohydride. The iron(II) complex (0.048 mmol, 4 mM) was placed in the cell, the mixture was stirred briefly, and the CV was performed immediately at a scan rate of 0.5 or 5 V s^{-1}. Sodium borohydride (0.048 mmol) was added, the mixture was stirred briefly, and the CV was performed immediately.

General Procedure C: Electrochemical Reduction of Iron Complexes in the Presence of Haloacetal. The iron complex (0.048 mmol, 4 mM) was placed in the cell, the mixture was stirred briefly, and the CV was performed immediately at a scan rate of 0.5 V s^{-1}. The haloacetal (0.048 mmol) was added, the mixture was stirred briefly, and the CV was performed immediately. Additional aliquots of haloacetal (1 equiv) were added, and the CV was performed immediately, up to a total of 4−12 equiv depending on substrate.

Mössbauer Spectroscopy. Mössbauer spectra were recorded on powder samples of natural-abundance ^{57}Fe compounds or on acetonitrile solutions starting with fully enriched $^{57}FeCl_2$ In the synthesis of isotopically enriched $^{57}FeCl_2$, elemental 94%-enriched ^{57}Fe was heated under a dry in situ generated chlorine atmosphere at 350 °C over 15 min. Dry chlorine was obtained by adding dropwise anhydrous sulfuric acid into a commercial bleach solution; the resulting chlorine gas was then dried by bubbling into sulfuric acid

DOI: 10.1021/acs.organomet.7b00603
Organometallics XXXX, XXX, XXX−XXX

(98%). The experiments were performed using a horizontal transmission 4 K closed cycle refrigerator system from Janis and SHI and a 100 mCi source of ^{57}Co(Rh) as previously described.[40] All velocity scales and isomer shifts are referred to the metallic iron standard at room temperature. Analysis of the data was performed with the software WMOSS4 Mössbauer spectral analysis software (www.wmoss.org, 2009−2015).

DFT Calculations. Simulations of the nuclear parameters were performed using the ORCA code (v. 3.0.3) at a DFT level (BP86, Ahlrich's TZVP set for all atoms except Fe, which was treated using the CP(PPP) set). See the Supporting Information for additional details and the corresponding references. Mössbauer parameters can be easily evaluated using straightforward DFT techniques, which allow the computation of the electronic density at the ^{57}Fe nucleus, denoted ρ_0 (in units of e a_0^{-3}, where a_0 is the Bohr radius). A reliable estimation of the isomer shift (δ) can be obtained with a linear extrapolation from ρ_0.[41] To do so, a benchmark of high-spin and low-spin Fe^{II} complexes has been used to calibrate the chosen level of theory. Computation of the quadrupolar split was not performed herein because this parameter is highly dependent on the symmetry of the occupied electronic levels. For several complexes in the following benchmark, the experimental value of ΔE_Q could not be reproduced with a satisfying accuracy. Minor differences between the optimized geometries and the experimental structures can induce strong discrepancies between the experimental and calculated values of ΔE_Q.[42] Computation of the Mössbauer parameters was performed using ORCA 3.0.3 software.[41] The BP86 functional[43] was used, with Ahlrich's TZVP basis set[44] for all atoms except Fe, which was described using the CP(PPP) enlarged basis set.[45]

■ ASSOCIATED CONTENT

Supporting Information

The Supporting Information is available free of charge on the ACS Publications website at DOI: 10.1021/acs.organomet.7b00603.

Experimental details and procedures, spectral data, electrochemical analysis, Mössbauer spectroscopy, and computational analysis (PDF)

■ AUTHOR INFORMATION

Corresponding Authors

*E-mail for L.F.: louis.fensterbank@upmc.fr.
*E-mail for A.J.: Anny.Jutand@ens.fr.
*E-mail for G.L.: Guillaume.Lefevre@cea.fr.
*E-mail for C.O.: cyril.ollivier@upmc.fr.

ORCID

Sara H. Kyne: 0000-0002-6995-9311
Etienne Derat: 0000-0002-8637-2707
Louis Fensterbank: 0000-0003-0001-7120
Guillaume Lefèvre: 0000-0001-9409-5861

Present Address

$^{\perp}$S.H.K.: School of Chemistry, University of Lincoln, Joseph Banks Laboratories, Lincoln LN6 7DL, U.K.

Notes

The authors declare no competing financial interest.

■ ACKNOWLEDGMENTS

The research leading to these results received funding from the European Union Seventh Framework Programme ([FP7/2007-2013]) under grant agreement n° [2988969] (S.H.K.). This work was also supported by the UPMC, ENS, CNRS, IUF (L.F.), ANR-10-BLAN-0701 CREDOX and ANR-12-BS07-0031 CoCaCoLight. Technical assistance was generously offered by FR 2769. Drs. Lise-Marie Chamoreau, Elsa Caytan, Denis Lesage, and Sébastien Blanchard are acknowledged for providing technical assistance and useful discussions.

■ REFERENCES

(1) Jahn, U.; Heinrich, M.; Gansäuer, A. *Top. Curr. Chem.* **2011**, *320*, 191−322.
(2) Kochi, J. K. *Acc. Chem. Res.* **1974**, *7*, 351−360.
(3) (a) Iqbal, J.; Bhatia, B.; Nayyar, N. K. *Chem. Rev.* **1994**, *94*, 519−564. (b) Gansäuer, A.; Bluhm, H. *Chem. Rev.* **2000**, *100*, 2771−2788.
(4) (a) Norton, J. R.; Sowa, J. *Chem. Rev.* **2016**, *116*, 8315−8317. and references cited therein (b) Jordan, A. J.; Lalic, G.; Sadighi, J. P. *Chem. Rev.* **2016**, *116*, 8318−8372.
(5) Takami, K.; Mikami, S.; Yorimitsu, H.; Shinokubo, H.; Oshima, K. *Tetrahedron* **2003**, *59*, 6627−6635.
(6) (a) Inoue, K.; Sawada, A.; Shibata, I.; Baba, A. *J. Am. Chem. Soc.* **2002**, *124*, 906−907. (b) Hayashi, N.; Shibata, I.; Baba, A. *Org. Lett.* **2004**, *6*, 4981−4983. (c) Baba, A.; Shibata, I. *Chem. Rec.* **2005**, *5*, 323−335.
(7) Fujita, K.; Nakamura, T.; Yorimitsu, H.; Oshima, K. *J. Am. Chem. Soc.* **2001**, *123*, 3137−3138.
(8) Liu, Y.; Schwartz, J. *Tetrahedron* **1995**, *51*, 4471−4482.
(9) (a) Kharasch, M. S.; Fields, E. K. *J. Am. Chem. Soc.* **1941**, *63*, 2316−2320. (b) Tamura, M.; Kochi, J. K. *J. Am. Chem. Soc.* **1971**, *93*, 1487−1489.
(10) Felkin, H.; Meunier, B. *Nouv. J. Chim.* **1977**, *1*, 281−282.
(11) (a) Hayashi, Y.; Shinokubo, H.; Oshima, K. *Tetrahedron Lett.* **1998**, *39*, 63−66. (b) For a review on iron-catalyzed hydrofunctionalization, see: Greenhalgh, M. D.; Jones, A. S.; Thomas, S. P. *ChemCatChem* **2015**, *7*, 190−222.
(12) (a) Freidlina, R. K.; Velichko, F. K. *Synthesis* **1977**, *1977*, 145−154. (b) Hilt, G.; Bolze, P.; Harms, K. *Chem. - Eur. J.* **2007**, *13*, 4312−4325. (c) Zhang, S.-Y.; Tu, Y.-Q.; Fan, C.-A.; Zhang, F.-M.; Shi, L. *Angew. Chem., Int. Ed.* **2009**, *48*, 8761−8765. (d) Prateeptongkum, S.; Jovel, I.; Jackstell, R.; Vogl, N.; Weckbecker, C.; Beller, M. *Chem. Commun.* **2009**, 1990−1992. (e) Vallée, F.; Mousseau, J.; Charette, A. B. *J. Am. Chem. Soc.* **2010**, *132*, 1514−1516. (f) Shirakawa, E.; Masui, S.; Narui, R.; Watabe, R.; Ikeda, D.; Hayashi, T. *Chem. Commun.* **2011**, *47*, 9714−9716. (g) Pratsch, G.; Anger, C. A.; Ritter, K.; Heinrich, M. *Chem. - Eur. J.* **2011**, *17*, 4104−4108. (h) Ito, S.; Itoh, T.; Nakamura, M. *Angew. Chem., Int. Ed.* **2011**, *50*, 454−457.
(13) For iron(II) or iron(III) hydride systems see: (a) Taniguchi, T.; Goto, N.; Nishibata, A.; Ishibashi, H. *Org. Lett.* **2010**, *12*, 112−115. (b) Leggans, E. K.; Barker, T. J.; Duncan, K. K.; Boger, D. L. *Org. Lett.* **2012**, *14*, 1428−1431. (c) Barker, T. J.; Boger, D. L. *J. Am. Chem. Soc.* **2012**, *134*, 13588−13591. (d) Lo, J. C.; Yabe, Y.; Baran, P. S. *J. Am. Chem. Soc.* **2014**, *136*, 1304−1307. (e) Lo, J. C.; Gui, J.; Yabe, Y.; Pan, C.-M.; Baran, P. S. *Nature* **2014**, *516*, 343−348. (f) Gui, J.; Pan, C.-M.; Jin, Y.; Qin, T.; Lo, J. C.; Lee, B. J.; Spergel, S. H.; Mertzman, M. E.; Pitts, W. J.; La Cruz, T. E.; Schmidt, M. A.; Darvatkar, N.; Natarajan, S. R.; Baran, P. S. *Science* **2015**, *348*, 886−891. (g) Dao, H. T.; Li, C.; Michaudel, Q.; Maxwell, B. D.; Baran, P. S. *J. Am. Chem. Soc.* **2015**, *137*, 8046−8049. (h) Lo, J. C.; Kim, D.; Pan, C.-M.; Edwards, J. T.; Yabe, Y.; Gui, J.; Qin, T.; Gutiérrez, S.; Giacoboni, J.; Smith, M. W.; Holland, P. L.; Baran, P. S. *J. Am. Chem. Soc.* **2017**, *139*, 2484−2503. (i) For a review on iron catalysis, see: Bauer, I.; Knölker, H.-J. *Chem. Rev.* **2015**, *115*, 3170−3387.
(14) Nakazawa, H.; Itazaki, M. *Top. Organomet. Chem.* **2011**, *33*, 27−81.
(15) (a) Marks, T. J.; Kolb, J. R. *Chem. Rev.* **1977**, *77*, 263−293. (b) Maity, A.; Teets, T. S. *Chem. Rev.* **2016**, *116*, 8873−8911.
(16) (a) Ekomié, A.; Lefèvre, G.; Fensterbank, L.; Lacôte, E.; Malacria, M.; Ollivier, C.; Jutand, A. *Angew. Chem., Int. Ed.* **2012**, *51*, 6942−6946. (b) Kyne, S. H.; Lévêque, C.; Zheng, S.; Fensterbank, L.; Jutand, A.; Ollivier, C. *Tetrahedron* **2016**, *72*, 7727−7737.
(17) Aresta, M.; Giannoccaro, P.; Rossi, M.; Sacco, A. *Inorg. Chim. Acta* **1971**, *5*, 115−118.
(18) Wulfsberg, G. In *Inorganic Chemistry*; University Science Books: Mill Valley, CA, 2000; pp 369−372.

DOI: 10.1021/acs.organomet.7b00603
Organometallics XXXX, XXX, XXX−XXX

(19) (a) Hathaway, B. J.; Holah, D. G. *J. Chem. Soc.* **1964**, *0*, 2408−2416. (b) Gao, Y.; Guery, J.; Jacoboni, C. *Acta Crystallogr., Sect. C: Cryst. Struct. Commun.* **1993**, *49*, 147−151. (c) Zhang, J.; Ensling, J.; Ksenofontov, V.; Gütlich, P.; Epstein, A. J.; Miller, J. S. *Angew. Chem., Int. Ed.* **1998**, *37*, 657−660. (d) Buschmann, W. E.; Miller, J. S. *Chem. - Eur. J.* **1998**, *4*, 1731−1737.
(20) Pokhodnya, K. I.; Bonner, M.; DiPasquale, A. G.; Rheingold, A. L.; Her, J.-H.; Stephens, P. W.; Park, J.-W.; Kennon, B. S.; Arif, A. M.; Miller, J. S. *Inorg. Chem.* **2007**, *46*, 2471−2477.
(21) Voloshin, Y. Z.; Varzatskii, O. A.; Kron, T. E.; Belsky, V. K.; Zavodnik, V. E.; Strizhakova, N. G.; Palchik, A. V. *Inorg. Chem.* **2000**, *39*, 1907−1918.
(22) Birchall, T.; Morris, M. F. *Can. J. Chem.* **1972**, *50*, 201−210.
(23) Gomez-Romero, P.; Witten, E. H.; Reiff, W. M.; Jameson, G. B. *Inorg. Chem.* **1990**, *29*, 5211−5217.
(24) Burger, K.; Horvàth, I. *Inorg. Chim. Acta* **1992**, *196*, 49−56.
(25) Burbridge, C. D.; Goodgame, D. M. L. *J. Chem. Soc. A* **1968**, *0*, 1410−1413.
(26) (a) Bancroft, G. M.; Mays, M. J.; Prater, B. E. *Chem. Phys. Lett.* **1969**, *4*, 248−250. (b) Itazaki, M.; Ito, M.; Nakashima, S.; Nakazawa, H. *Dalton Trans.* **2016**, *45*, 1327−1330.
(27) Pokhodnya, K. I.; Bonner, M.; DiPasquale, A. G.; Rheingold, A. L.; Miller, J. S. *Chem. - Eur. J.* **2008**, *14*, 714−720.
(28) Schmid, R.; Kirchner, K.; Dickert, F. L. *Inorg. Chem.* **1988**, *27*, 1530−1536.
(29) Glavee, G. N.; Klabunde, K. J.; Sorensen, C. M.; Hadjipanayis, G. C. *Inorg. Chem.* **1995**, *34*, 28−35.
(30) (a) Schaeffer, G. W.; Roscoe, J. S.; Stewart, A. C. *J. Am. Chem. Soc.* **1956**, *78*, 729−733. (b) Monnier, G. *Ann. Chim. (Paris)* **1957**, *2*, 14.
(31) (a) For a review on the different possible coordination modes of borohydride anion with transition and f-block metals, see: Marks, T. J.; Kolb, J. R. *Chem. Rev.* **1977**, *77*, 263−293. (b) Baker, M. V.; Field, L. D. *Appl. Organomet. Chem.* **1990**, *4*, 543−549. (c) Langer, R.; Iron, M. A.; Konstantinovski, L.; Diskin-Posner, Y.; Leitus, G.; Ben-David, Y.; Milstein, D. *Chem. - Eur. J.* **2012**, *18*, 7196−7209. (d) Koehne, I.; Schmeier, T. J.; Bielinski, E. A.; Pan, C. J.; Lagaditis, P. O.; Bernskoetter, W. J.; Takase, M. K.; Würtele, C.; Hazari, N.; Schneider, S. *Inorg. Chem.* **2014**, *53*, 2133−2143.
(32) Alberico, E.; Sponholz, P.; Cordes, C.; Nielsen, M.; Drexler, H.-J.; Baumann, W.; Junge, H.; Beller, M. *Angew. Chem., Int. Ed.* **2013**, *52*, 14162−14166.
(33) Kuhn, N.; Kotowski, H.; Maichle-Mößmer, C.; Abram, U. *Z. Anorg. Allg. Chem.* **1998**, *624*, 1653−1656.
(34) The weak coordination of the borohydride anion to the metal leads under these conditions leads to the observation of the $[M-BH_4]^+$ fragment. For an example, see ref 31a.
(35) Other structures such as $[(\eta^1\text{-}H_3BH)Fe(NCCH_3)_5]^+$ also led to computed nuclear parameters comparable with the experimental data; however, these species were found to be much less stable than the complexes given in Scheme 8 and Table 3 (see the Supporting Information).
(36) For a discussion about the potential gap that allows a single electron transfer see: Enemærke, R. J.; Christensen, T. B.; Jensen, H.; Daasbjerg, K. *J. Chem. Soc. Perkin Trans. 2* **2001**, 1620−1630.
(37) (a) Abeywickrema, A. N.; Beckwith, A. L. J. *Tetrahedron Lett.* **1986**, *27*, 109−112. (b) Kropp, M.; Schuster, G. B. *Tetrahedron Lett.* **1987**, *28*, 5295−5298. (c) Liu, Q.; Han, B.; Zhang, W.; Yang, L.; Liu, Z.-L.; Yu, W. *Synlett* **2005**, 2248−2250. (d) Kobayashi, S.; Kawamoto, T.; Uehara, S.; Fukuyama, T.; Ryu, I. *Org. Lett.* **2010**, *12*, 1548−1551. (e) For a recent review on borohydride-mediated radical reactions, see: Kawamoto, T.; Ryu, I. *Org. Biomol. Chem.* **2014**, *12*, 9733−9742.
(38) Lee, J.-G.; Jung, G.-S.; Lee, S. W. *Bull. Korean Chem. Soc.* **1998**, *19*, 267−369.
(39) Pokhodnya, K. I.; Bonner, M.; DiPasquale, A. G.; Rheingold, A. L.; Her, J.-H.; Stephens, P. W.; Park, J.-W.; Kennon, B. S.; Arif, A. M.; Miller, J. S. *Inorg. Chem.* **2007**, *46*, 2471−2477.
(40) Gouré, E.; Thiabaud, G.; Carboni, M.; Gon, N.; Dubourdeaux, P.; Garcia-Serres, R.; Clémancey, M.; Oddou, J.-L.; Robin, A. Y.; Jacquamet, L.; Dubois, L.; Blondin, G.; Latour, J.-M. *Inorg. Chem.* **2011**, *50*, 6408−6410.
(41) Neese, F. The ORCA program system. *Comput. Mol. Sci.* **2012**, *2*, 73−78.
(42) Pàpai, M.; Vankò, G. *J. Chem. Theory Comput.* **2013**, *9*, 5004−5020.
(43) (a) Becke, A. D. *Phys. Rev. A: At., Mol., Opt. Phys.* **1988**, *38*, 3098−3100. (b) Perdew, J. P. *Phys. Rev. B: Condens. Matter Mater. Phys.* **1986**, *33*, 8822−8824.
(44) Schafer, A.; Huber, C.; Ahlrichs, R. J. *J. Chem. Phys.* **1994**, *100*, 5829−5835.
(45) (a) Neese, F. *Inorg. Chim. Acta* **2002**, *337*, 181−192. (b) Sinnecker, S.; Slep, L. D.; Bill, E.; Neese, F. *Inorg. Chem.* **2005**, *44*, 2245−2254.

DOI: 10.1021/acs.organomet.7b00603
Organometallics XXXX, XXX, XXX−XXX